iScience

CellPress
OPEN ACCESS

Article

Chronic AMPK inactivation slows SHH medulloblastoma progression by inhibiting mTORC1 signaling and depleting tumor stem cells

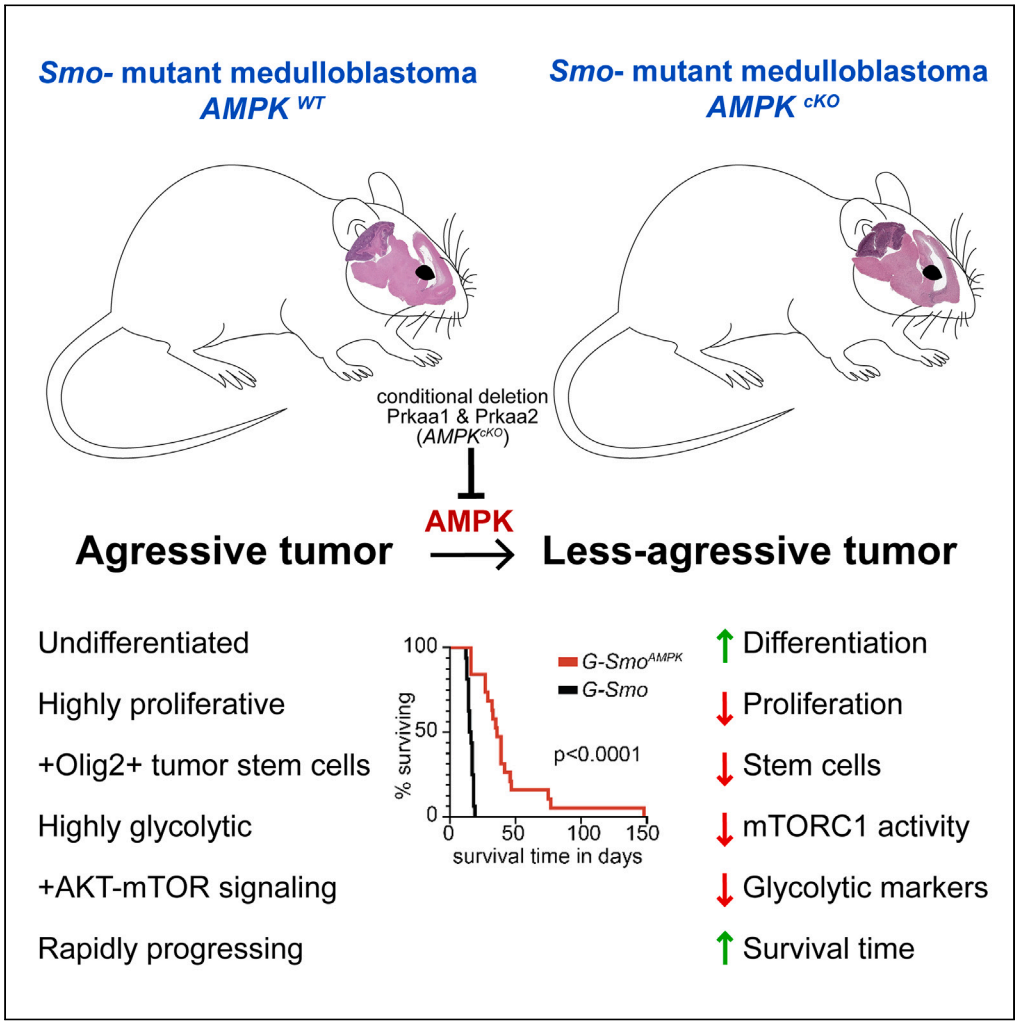

Daniel Shiloh Malawsky, Taylor Dismuke, Hedi Liu, ..., Biplab Dasgupta, Andrey Tikunov, Timothy R. Gershon

timothy.gershon@emory.edu

Highlights

Genetic AMPK inactivation slows tumor progression in SHH medulloblastoma in mice

AMPK-deleted tumors show increased differentiation and reduced proliferation

Disabling AMPK reduces mTORC1 activity and HK2-dependent glycolysis

AMPK inactivation disproportionately impairs medulloblastoma stem cell populations

Malawsky et al., iScience 26, 108443
December 15, 2023
https://doi.org/10.1016/j.isci.2023.108443

iScience

CellPress
OPEN ACCESS

Article

Chronic AMPK inactivation slows SHH medulloblastoma progression by inhibiting mTORC1 signaling and depleting tumor stem cells

Daniel Shiloh Malawsky,[1,6] Taylor Dismuke,[1,6] Hedi Liu,[1] Ethan Castellino,[2] Jay Brenman,[3] Biplab Dasgupta,[4] Andrey Tikunov,[1,2,5] and Timothy R. Gershon[1,2,5,7,*]

SUMMARY

We show that inactivating AMPK in a genetic medulloblastoma model depletes tumor stem cells and slows progression. In medulloblastoma, the most common malignant pediatric brain tumor, drug-resistant stem cells co-exist with transit-amplifying cells and terminally differentiated neuronal progeny. Prior studies show that *Hk2*-dependent glycolysis promotes medulloblastoma progression by suppressing neural differentiation. To determine how the metabolic regulator AMPK affects medulloblastoma growth and differentiation, we inactivated AMPK genetically in medulloblastomas. We bred conditional *Prkaa1* and *Prkaa2* deletions into medulloblastoma-prone *SmoM2* mice and compared *SmoM2*-driven medulloblastomas with intact or inactivated AMPK. AMPK-inactivation increased event-free survival (EFS) and altered cellular heterogeneity, increasing differentiation and decreasing tumor stem cell populations. Surprisingly, AMPK-inactivation decreased mTORC1 activity and decreased *Hk2* expression. *Hk2* deletion similarly depleted medulloblastoma stem cells, implicating reduced glycolysis in the AMPK-inactivated phenotype. Our results show that AMPK inactivation disproportionately impairs medulloblastoma stem cell populations typically refractory to conventional therapies.

INTRODUCTION

Medulloblastoma is the most common malignant pediatric brain tumor and recurrence after treatment is the major cause of morbidity for patients with medulloblastoma. Medulloblastoma, is a heterogeneous group of cancers with 4 major subgroups, each with different recurrence risk,[1–4] and individual tumors in each subgroup show cellular heterogeneity.[5,6] Cellular heterogeneity may contribute to recurrence by increasing overall robustness to overcome selective pressures of therapy, and by generating specific resistant populations that drive recurrence. Understanding how different conditions affect the diversity of cell types within medulloblastomas is critical to designing therapies that can reduce the chance of recurrent disease. We previously showed that disrupting energy metabolism by conditionally deleting *Hk2* in transgenic SHH medulloblastoma-prone mice slowed tumor progression and increased differentiation.[7] These data show that metabolic patterns regulate clinically relevant aspects of medulloblastoma phenotype. Here, we examine how reducing metabolic adaptability alters medulloblastoma growth by disabling the intracellular energy sensor AMP-activated kinase (AMPK) in a genetic mouse model of SHH medulloblastoma. We then compare the phenotype of tumors with AMPK inactivation or *Hk2* deletion.

SHH (Sonic Hedgehog) subgroup tumors, the most frequent subgroup of medulloblastoma, can be recapitulated in mice genetically engineered to hyperactivate SHH signaling in the brain, producing tumors that resemble human SHH medulloblastoma in site, pathology, gene expression, and cellular heterogeneity.[5,8,9] Studies of SHH-driven medulloblastomas in mice show that cellular heterogeneity contributes to tumor recurrence as individual cell types within tumors show different sensitivity or resistance to specific therapies and cells that survive treatment drive recurrence.[10,11] Tumor stem cells, marked by the expression of OLIG2, are specifically resistant to cytotoxic treatments currently used in medulloblastoma therapy and initiate post-treatment recurrence.[10] Currently, 20% of patients with SHH subgroup medulloblastoma experience incurable recurrence despite optimal up-front therapy. Identifying ways to target therapy-resistant tumor stem cells may allow conventional treatment to be effective for more patients.

[1]Department of Neurology, University of North Carolina School of Medicine, Chapel Hill, NC 27599, USA
[2]Department of Pediatrics, Emory University School of Medicine, Atlanta, GA 30322, USA
[3]Department of Cell Biology and Physiology, University of North Carolina School of Medicine, Chapel Hill, NC 27599, USA
[4]Division of Oncology, Cincinnati Children's Hospital Medical Center, Cincinnati, OH 45229, USA
[5]Children's Center for Neurosciences Research, Children's Hospital of Atlanta, Emory University, Atlanta, GA 30322, USA
[6]These authors contributed equally
[7]Lead contact
*Correspondence: timothy.gershon@emory.edu
https://doi.org/10.1016/j.isci.2023.108443

Tumor cells in medulloblastoma show a range of differentiation states that reflect the developmental progression in cerebellar development: from undifferentiated stem cells to committed cerebellar granule neuron progenitors (CGNPs) to differentiated neurons, including unipolar brush cells (UBCs) and cerebellar granule neurons (CGNs).[12] However, medulloblastomas also contain tumor-derived cells with glial differentiation, and this divergence from the neural lineage of CGNPs provides indirect evidence of medulloblastoma stem cells with glio-neuronal potency.[11,13]

AMPK is a multi-subunit complex that is a primary regulator of cellular energy homeostasis,[14] and disrupting AMPK function may produce important anti-tumor effects.[15] AMPK-mediated coordination of energy metabolism may be particularly important in SHH medulloblastomas, because SHH induces specialized metabolic features that support malignant growth,[16] including HK2-dependent aerobic glycolysis,[7,17] lipogenesis,[18] HIF1α stabilization[19] and mitochondrial fragmentation.[20] These metabolic adaptations may increase the need for AMPK to sense energy scarcity in order to maintain energy homeostasis.

While AMPK is activated by the tumor suppressor LKB1, many lines of evidence show that the role of AMPK in cancer is more complex [20]. In contrast to the multiple inactivating LKB1 mutations that have been found in diverse human cancers,[21–23] mutations in AMPK subunits causing human cancer are unknown. Divergent roles of LKB1 and AMPK are demonstrated by the $Kras^{G12D}$ mouse lung tumor model, in which *Lkb1* deletion accelerates tumor growth while the co-deletion of the two AMPK catalytic subunits *Prkaa1* and *Prkaa2* inhibits tumorigenesis.[24] Apart from operating downstream of LKB1, numerous studies show that AMPK functions to increase metabolic adaptability in normal cells within the brain.[25,26] AMPK-mediated metabolic adaptability may be advantageous to brain tumors.[27,28] Importantly, AMPK can be inactivated in the mouse brain or whole body without producing discernable developmental abnormalities.[28–30] While chronic, sustained AMPK inactivation through *Prkab1/1* co-deletion in astrocytes results in neurodegeneration in aged mice,[26] therapies that transiently disrupt AMPK may be safe in pediatric patients with medulloblastoma.[28,31]

Prior studies show that AMPK acts in medulloblastoma to support tumor growth, as the deletion of *Prkaa2*, the gene encoding the AMPKα2 catalytic domain slows tumor progression in mice engineered to develop SHH-driven medulloblastoma.[31] One process contributing to this effect is loss of AMPK-mediated phosphorylation of the zinc finger protein CNBP, which decreases the translation of Ornithine Decarboxylase (ODC) and the production of polyamines.[31,32] However, the mechanisms through which polyamine production permits tumor growth are unresolved, and other AMPK-dependent mechanisms may also affect medulloblastoma growth. The repertoire of glycolytic genes expressed by medulloblastoma cells changes with differentiation state,[7,16,17] and this variation suggest that specific types of tumor cells within medulloblastomas may depend on AMPK for different purposes.

To resolve AMPK function in different tumor cell subpopulations within medulloblastomas, we investigated the consequence of AMPK catalytic domain ablation through *Prkaa1 and Prkaa2* co-deletion in medulloblastomas driven by oncogenic, mutant *Smo*. We used scRNA-seq and IF to examine the impact of AMPK inactivation on different types of cells within medulloblastomas, and compared to *Hk2*-deleted medulloblastomas to probe the mechanistic role of altered metabolism. Our studies show that *Prkaa1/Prkaa2* co-deletion, such as *Hk2* deletion, increased intra-tumoral differentiation. Notably, *Prkaa1/Prkaa2* co-deletion reduced the populations of OLIG2-expressing stem cells that drive recurrence after conventional therapy. These studies provide new mechanistic insight into how metabolic specialization supports the diverse communities of tumor cells that promote recurrence after therapy.

RESULTS

AMP-activated kinase signaling in Sonic Hedgehog medulloblastoma

To investigate a potential dependence of medulloblastoma on AMPK, we analyzed publicly available data from medulloblastomas resected from patients[33] using the R2: Genomics Analysis and Visualization Platform (http://r2.amc.nl). We did not find a statistically significant effect of *PRKAA1* or *PRKAA2* expression on overall survival in any subgroup. However, while *PRKAA1* and *PRKAA2* expression were variable in each subgroup, SHH subgroup medulloblastomas showed significantly higher *PRKAA1* expression compared to each of the other tumor types (Figure 1A). The subgroup-specific tendency for increased *PRKAA1* expression suggested a role for AMPK activity in the growth of SHH medulloblastomas.

AMP-activated kinase inactivation in medulloblastomas increase survival of tumor-bearing mice

To test the importance of AMPK function in SHH medulloblastoma experimentally, we generated medulloblastoma-prone mice with CNS-specific *Prkaa1/Prkaa2* co-deletion. We intercrossed *Gfap-Cre* mice that express Cre recombinase in CNS stem cells during development with $Prkaa1^{loxP/loxP}/Prkaa2^{loxP/loxP}$[29] and *SmoM2*[34] mouse lines to generate $Gfap\text{-}Cre/Prkaa1^{loxP/loxP}/Prkaa2^{loxP/loxP}/SmoM2$ ($G\text{-}Smo^{AMPK}$) mice with brain-wide, Cre-conditional AMPK inactivation, and brain-wide, Cre-conditional SHH hyperactivation.

SHH hyperactivation in *Gfap-Cre/SmoM2* (*G-Smo*) mice produces medulloblastoma with 100% penetrance by postnatal day 10 (P10) and no other brain tumors.[35] Similar to *G-Smo* mice, all $G\text{-}Smo^{AMPK}$ mice developed medulloblastoma that was detectable by characteristic change in head shape at P10 and resembled *G-Smo* medulloblastoma in site and overt pathology, as in representative samples taken at P16 (Figures 1B and 1C). In the absence of treatment, all *G-Smo* mice die of tumor progression by P22.[7,36] In contrast, untreated $G\text{-}Smo^{AMPK}$ mice showed significantly longer survival times, with a median survival of 44 days in $G\text{-}Smo^{AMPK}$ compared to 16 days in controls ($p < 0.0001$ by Log-Rank test; Figure 1D). These data show that AMPK inactivation in the *G-Smo* model did not prevent medulloblastoma formation, but impaired medulloblastoma progression. The reduced medulloblastoma growth is consistent with prior studies in which isolated *Prkaa2* deletion reduced tumorigenesis in an SHH medulloblastoma model driven by the *SmoA1* allele.[31] Considering the consistent tumor-suppressive

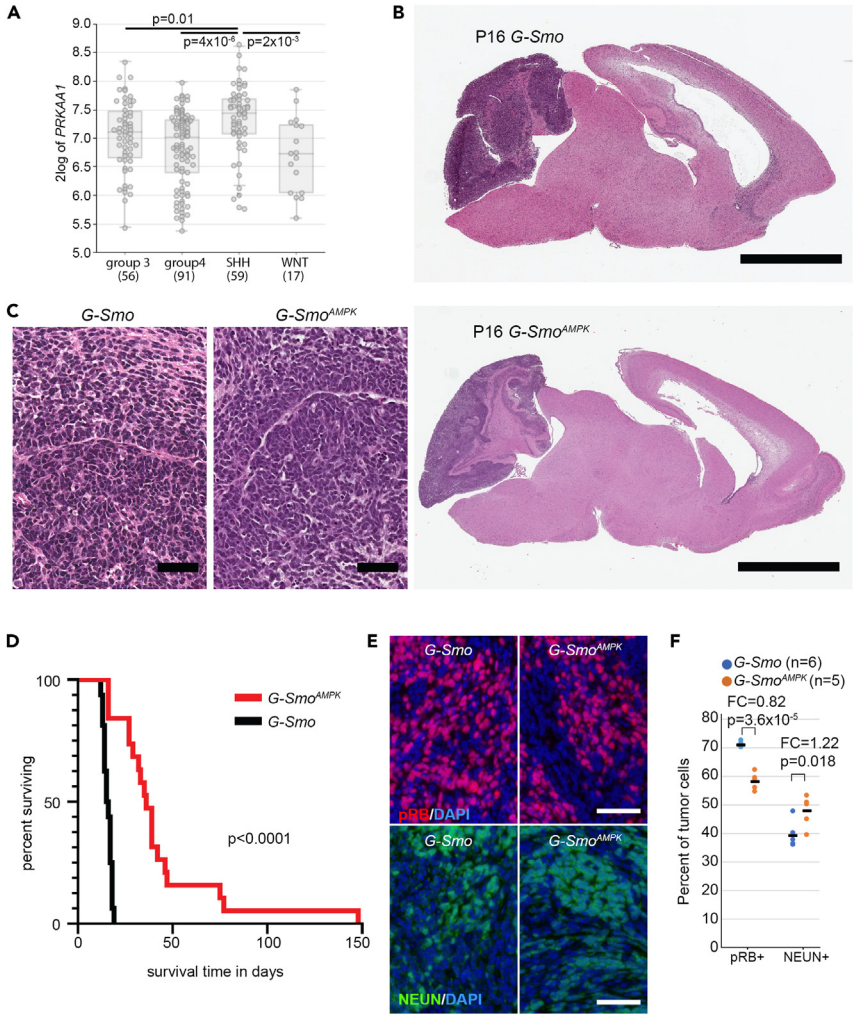

Figure 1. AMPK inactivation slows the progression of SHH-driven medulloblastoma

(A) *PRKAA1* mRNA expression in clinical medulloblastoma samples of indicated subgroups, p values determined by 1-way ANOVA comparing the indicated pairs. In this box and whiskers plot, boxes indicate the upper and lower quartiles, the horizontal line between boxes indicates the mean, and whiskers inidcate 150% of the interquartile range, limited by the total range.

(B and C) Representative sagittal brain sections from *G-Smo* and *G-Smo*^{AMPK} mice show similar site of tumor formation and hypercellular tumor pathology.

(D) Increased survival time in *G-Smo*^{AMPK} mice compared to *G-Smo* controls with intact AMPK. Survival times in (D) were compared by Log-Rank test.

(E) Representative IF on sagittal sections of *G-Smo* and *G-Smo*^{AMPK} medulloblastomas, showing pRB and NEUN expression.

(F) Quantification of the fractions of tumor cells expressing the indicated marker in 6 replicate *G-Smo* tumors and 5 replicate *G-Smo*^{AMPK} tumors of each genotype, compared by Student's *t* test. Bars = 3 mm in (B) and 50 μm in (C and E).

effect of AMPK inactivation in multiple SHH medulloblastoma models, we studied the changes in growth parameters and cellular heterogeneity in AMPK-inactivated tumors.

We analyzed the populations of replicate *G-Smo*^{AMPK} mice and *G-Smo* controls undergoing proliferation, differentiation, and apoptosis. In medulloblastomas from both genotypes harvested at P15, we compared the fractions of cells expressing the proliferation marker phosphorylated RB (pRB), the differentiation marker NEUN, and the apoptosis marker cleaved Capase-3 (cC3; Figure 1E; Figures S1A–S1C). pRB and NEUN showed complementary patterns of regional variation, distinguishing regions with more proliferation from regions with more differentiation (Figures S1A and S1B). *G-Smo*^{AMPK} medulloblastomas showed significantly lower proliferation index, (defined as pRB+ cells/total cells, $p = 3.6x10^{-5}$, compared by Student's *t* test; fold change (FC) = 0.82) and significantly higher differentiation index (defined as NEUN+ cells/total cells, p = 0.018, compared by Student's *t* test; FC = 1.22) (Figure 1F). In contrast, the apoptotic rate trended higher in the *G-Smo*^{AMPK} tumors with increased variability compared to controls, but was not significantly different when compared by Student's *t* test (Figures S1C and S1D). These findings implicate decreased proliferation and increased differentiation rather than increased apoptosis in the slower progression of AMPK-inactivated tumors.

AMP-activated kinase inactivation alters medulloblastoma cellular heterogeneity and induces differentiation

To resolve changes in cellular heterogeneity within the AMPK-inactivated and control tumors, we used scRNA-seq to compare tumors from 4 replicate P15 *G-Smo*^{AMPK} mice to 6 medulloblastomas from replicate P15 *G-Smo* controls. We processed tumors using Drop-seq and generated cell-specific, bar-coded sequencing data, using our published methods.[11,37–39] We filtered putative cells, identified by bead-specific barcodes, to address the common problems of gene drop out, unintentional cell-cell multiplexing and premature cell lysis.[40] 53% of putative cells from *G-Smo* mice and 43% of putative *G-Smo*^{AMPK} cells met QC criteria and were included in the analysis resulting in 11,203 cells across 6 *G-Smo* replicates and 2426 cells across 4 *G-Smo*^{AMPK} replicates. To compare the two genotypes at similar sequencing depths, we randomly down-sampled the *G-Smo* transcript counts to 46.5% of the original depth.[41]

We used the Harmony algorithm to integrate the scRNA-seq data from *G-Smo*^{AMPK} and *G-Smo* tumors in a single analysis, generating a 2-dimensional UMAP projection in which individual cells were clustered with cells of similar gene expression. As in prior studies, this analysis defined both discrete clusters and a group of clusters with shared borders (Figure 2A). Individual replicates from each genotype distributed evenly across the UMAP (Figure S2). We determined the biological relevance of the clusters by generating cluster-specific differential gene expression profiles, comparing the expression by cells within the cluster to the expression by all cells outside the cluster (Data S1). These gene expression profiles identified the cell type of each cluster. The full set of gene expression data with single cell resolution from *G-Smo*^{AMPK} and *G-Smo* control tumors can be viewed at: https://malawsky.shinyapps.io/Gerhson_AMPK_analysis.

As in our prior studies, these methods identified each of the discrete clusters as different types of stromal cells typical of brain tissue. We thus identified astrocytes, oligodendrocytes, ependymal cells, myeloid cells, endothelial cells and fibroblasts (Table 1; Figure 2A). The cluster-specific gene expression patterns identified the multi-cluster aggregate as medulloblastoma cells in a range of states that paralleled CGNP development, from proliferative and undifferentiated to non-proliferative at different stages of neural differentiation (Table 1).

The expression of the CGNP marker *Barhl1*[42] and the CGN differentiation marker *NeuroD1*[43] divided the multi-cluster aggregate into two adjacent, mutually exclusive domains, consisting of *Barhl1+* clusters 0, 2, 3, 5, 7 expressed and *NeuroD1+* clusters 1,4 and 6 (Figure 2B). Similarly, hierarchical clustering using the expression of a panel of genes associated with either cell cycling (*Mki67*, *Pcna*, *Top2a*, *Ccnd1* and SHH pathway transcription factor Gli1) or neural differentiation (*Rbfox3*, *Neurod1*, *Cntn2* and *Tubb3*) divided clusters 0, 2, 3, 5, 7, and clusters 1,4 and 6 into distinct groups (Figure 2C). Uniformly decreased expression of proliferation markers and increased expression of neural markers identified clusters 1,4 and 6 as non-proliferative and differentiating. In contrast, increased expression of heterogeneous combinations of proliferation markers identified Clusters 0, 2, 3, 5, 7, and 8 as proliferative.

We compared the fractions of differentiating cluster populations (summed populations of clusters 1, 4, and 6) in each replicate *G-Smo* or *G-Smo*^{AMPK} animal, using the Student's *t* test. *G-Smo*^{AMPK} tumors showed significantly increased fractions of differentiating cells, and reciprocally decreased proliferating cells. IF studies confirmed significantly fewer cells expressing KI67 protein in *G-Smo*^{AMPK} tumors (Figures 2D and 2E) and significantly more cells expressing NEUROD1 protein (Figures 2F and 2G) compared to controls. These studies confirm that AMPK inactivation shifted the balance between proliferation and differentiation in *G-Smo*^{AMPK} tumors toward differentiation, consistent with increased NEUN and decreased pRB.

We disaggregated the cells by genotype to compare the populations and gene expression patterns of the type of cell in *G-Smo*^{AMPK} and *G-Smo* control tumors. In view of the inter-relation between populations normalized cluster populations, we used Dirichlet regression to make statistical comparisons of stromal cluster populations in *G-Smo*^{AMPK} tumors versus controls (Figure 2H).[44] Most stromal populations did not show significant differences between genotypes, including astrocytes and myelinating oligodendrocytes which were both within the GFAP lineage and thus subject to *Prkaa1/2* deletion. However, immature oligodendrocytes (Cluster 10), which were within the GFAP lineage and thus also subject to *Prkaa1/2* deletion, were markedly less numerous in *G-Smo*^{AMPK} tumors ($p = 0.02$; FC = 0.33). Additionally, *G-Smo*^{AMPK} tumors showed a marked increase in endothelial cells ($p = 0.02$; FC = 3.40), which are not within the GFAP lineage and therefore were not *Prkaa1/2*-deleted. AMPK inactivation thus increased differentiation in both the tumor and oligodendrocyte lineages and also produced a non-cell autonomous increase in endothelial cells.

AMP-activated kinase-inactivated medulloblastomas show reduced OLIG2+ stem cells

Considering increased differentiation in AMPK-inactivated medulloblastomas and extended survival time, we determined if tumor stem cell populations, which remain undifferentiated and play an essential role in medulloblastoma progression, were reduced. We compared the populations of tumor cells that expressed the stem cell markers *Hes1*, *Olig2*, *Sox2*, and *Vim* in *G-Smo* versus *G-Smo*^{AMPK} tumors. To focus on tumor stem cells, we excluded stromal cells, as astrocytes express *Hes1* and *Sox2*, oligodendrocytes express *Sox2* and *Olig2*, and diverse stromal cells express *Vim*. *G-Smo*^{AMPK} medulloblastomas showed significantly fewer *Olig2+* cells (FC = 0.43, $p = 0.0025$ by Student's *t* test) and *Vim+* cells (FC = 0.52, $p = 0.0011$ by Student's *t* test) (Figures 3A and 3B). Similarly, *Sox2+* cells and *Hes1+* cells showed trends toward reduced numbers that were not statistically significant (FC = 0.90, $p = 0.67$ and FC = 0.82 $p = 0.15$), within the statistical power of the study.

To compare stem cell populations using an alternative detection method, we analyzed OLIG2 protein expression, detected by IF. As both tumor stem cells and oligodendrocytes express OLIG2, we used the oligodendrocyte marker SOX10 to distinguish between these two cell types, considering OLIG2+/SOX10-cells in medulloblastomas as tumor stem cells. These OLIG2+/SOX10-stem cells were increased in perivascular regions (Figure 3B), consistent with prior descriptions of medulloblastoma stem cells.[45,46] The fractions of OLIG2+/SOX10-cells were markedly reduced in *G-Smo*^{AMPK} tumors (Figures 3C and 3D; $p = 0.002$; FC = 0.29; Student's *t* test), consistent with the differences in *Olig2+* populations in the tumor cell populations isolated and analyzed in the scRNA-seq data. The scRNA-seq data on *Olig2* mRNA expression and the IF studies of OLIG2 protein consistently demonstrate decreased *Olig2*-expressing stem-like populations in AMPK-inactivated medulloblastomas.

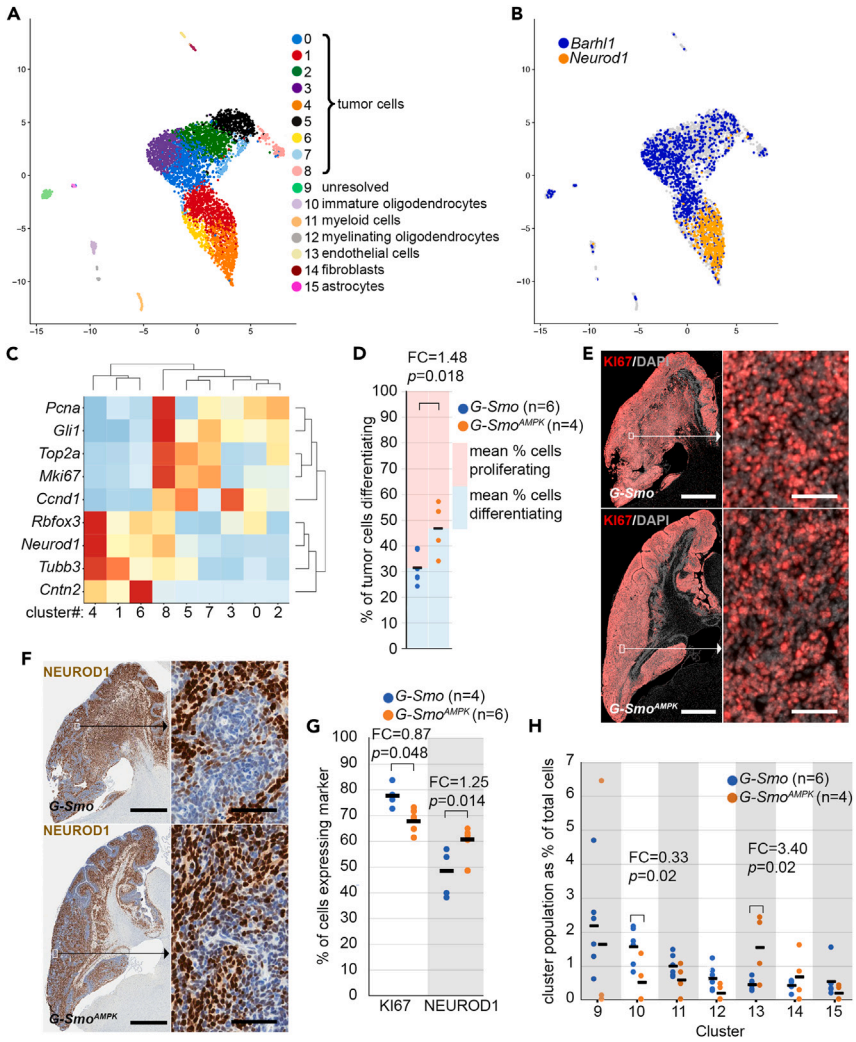

Figure 2. AMPK inactivation alters cellular heterogeneity in SHH driven medulloblastomas

(A) UMAP plot of all cells from *G-Smo* and *G-Smo*^{AMPK} tumors, color-coded by cluster. Cells are localized according to their proximity in PCA space.

(B) Feature plot showing the expression of *Barhl1* and *Neurod1*, color coded over the UMAP shown in (A).

(C) Heatmap showing the scaled expression of indicated genes in each tumor cell cluster. Hierarchical clustering of genes appropriately grouped the proliferation markers and differentiation markers into two discrete sets. Hierarchical clustering of clusters 0–8 grouped the clusters into two discrete sets that corresponded with the expression of differentiation and proliferation markers.

(D) Comparison between genotypes of the fractions of differentiation tumor cells (Clusters 1, 4 and 6) from each replicate. The blue and red regions show the mean % differentiating and reciprocal % proliferating, indicating the balance between proliferation and differentiation within each genotype.

(E and F) Representative (E) KI67 IF and (F) NEUROD1 IHC, on sagittal sections of *G-Smo* and *G-Smo*^{AMPK} medulloblastomas.

(G) Comparison of the fractions of tumor cells from each replicate expressing KI67 and NEUROD1.

(H) Comparison of populations of each stromal cluster in *G-Smo* and *G-Smo*^{AMPK} tumors. In panels (D), (G) and (H), horizontal bars indicate the mean values for the conditions, dots represent values for individual replicates, and the number of visible dots may be smaller than the sample size (n) due to multiple replicates showing similar values. In (D) and (G), Student's *t* test was used to make pairwise comparisons. In (H), Dirichlet regression was used to make statistical comparisons. In panels (E) and (F), bars = 1 mm in the left panel and 25 μm in the right panel.

AMP-activated kinase-inactivation disrupts tumor to glia *trans*-differentiation

Lineage tracing in mouse models of SHH medulloblastoma show that tumor cells *trans*-differentiate to generate tumor-derived glial populations,[11,13] and that these malignant glial cells play a supportive role in tumor growth.[13] Glial *trans*-differentiation requires stem-like pluripotency, and in light of the reduced stem-like population in *G-Smo*^{AMPK} tumors, we compared glial *trans*-differentiation in *G-Smo*^{AMPK} and *G-Smo* control tumors.

We traced lineage in the scRNA-seq data using the 3′ *Yfp* sequence in the *Cre*-conditional *SmoM2* transgene. We previously used this method to show that some astrocytes and oligodendrocytes derive from the tumor lineage in medulloblastomas that form in *Math1-Cre/SmoM2* mice.[11]

Table 1. Identification of clusters as specific types of tumor and stromal cells

Cluster	Cell type designation	distinctive markers	Tumor cell classification
0	tumor cells	*Barhl1*	proliferative
1	early differentiating tumor cells	*Tubb3, Stmn2*	differentiating
2	proliferating tumor cells	*Top2a, Dek*	proliferative
3	tumor cells	*Gas5, Rps20*	proliferative
4	differentiating tumor cells	*Stmn2, Celf4, Nrxn1*	differentiating
5	mitotic tumor cells	*Cenpa, Ube2c*	proliferative
6	late differentiating tumor cells	*Cntn2, Gria2, Apc*	differentiating
7	proliferating tumor cells	*Top2a, Mki67*	proliferative
8	proliferating tumor cells	*Top2a, Mki67, Ube2c*	proliferative
9	unresolved	*Mt1, Mt2*	stromal
10	immature oligodendrocytes	*Olig1/2, Pdgfra*	stromal
11	myeloid cells	*C1qc/a, Tyrobp*	stromal
12	myelinating oligodendrocytes	*Plp1, Mbp*	stromal
13	endothelial cells	*Cldn5*	stromal
14	fibroblasts	*Dcn*	stromal
15	astrocytes	*Aqp4, Slc1a3*	stromal

In the *G-Smo* control tumors, we found *SmoM2-Yfp*+ cells in the astrocytic cluster 15 and in the oligodendrocytic clusters 10 and 12. The detection of the *Yfp* tag in astrocytes and oligodendrocytes was expected since *Gfap-Cre* activates *SmoM2* in glio-neuronal stem cells of the developing brain that generate both glial and neuronal progeny. However, not all glia were *SmoM2-Yfp*+, indicating that *SmoM2* activation was not uniform in these populations. We therefore considered that tumor-derived glia contributed to the *Yfp*+ glial populations and used the variation glial *Yfp* expression to compare the glial cells of tumor lineage between genotypes. *G-Smo*^{AMPK} tumors showed significantly smaller *SmoM2-Yfp*+ glial populations, indicating fewer tumor-derived glia (Figure 3E, p = 0.024; FC = 0.18; Student's *t* test). This evidence for decreased glial *trans*-differentiation suggests that the tumor stem cell pluripotency that allows glial differentiation within medulloblastomas was reduced in *G-Smo*^{AMPK} tumors. However, it is also possible that *Prkaa1/2*-deleted glia were less able to tolerate *SmoM2* expression, and this alternative possibility may also explain the variation in *Yfp*-tagged glia between genotypes.

Decreased mTORC1 activation in AMP-activated kinase-inactivated medulloblastomas

To identify molecular pathways altered by AMPK inactivation, we defined the set of genes that were differentially expressed in *G-Smo*^{AMPK} tumors compared to *G-Smo* control tumors. We analyzed DEGs in the combined set of all tumor cells (Clusters 0–8), and in each separate cluster. Analyzing DEGs within each cluster controlled for differences in the distribution of tumor cells across clusters populations in the two genotypes, and analyzing DEGs that recurred in multiple clusters identified changes in gene expression the were common across cells in multiple states. For these analyses we identified DEGs that showed a corrected p value of <0.05 (Wilcoxon rank-sum test).

Comparing all tumor cells in *G-Smo*^{AMPK} mice versus *G-Smo* controls, we identified 64 DEGs, 34 up-regulated in *G-Smo*^{AMPK} and 30 down-regulated (Data S1). Of these 64 DEGs, 25 were ribosomal genes and 30 were within the broader set of genes ribonucleoprotein complex ($p = 2.39x10^{-37}$ and $9.84x10^{-27}$ by PANTHER Overrepresentation Test using the GO cellular component complete dataset). Consistent with high ribosomal association, gene set enrichment analysis (GSEA) identified translation as the most prominently enriched cellular process (p = 0.00032 by GSEA) (Figure 4A). PANTHER Overrepresentation Test using the GO biologic process complete dataset demonstrated that genes down-regulated in *G-Smo*^{AMPK} tumors were more strongly associated with translation, with 6/34 up-regulated genes associated with translation (p > 0.05) compared to 20/30 down-regulated genes ($p = 5.22 \times 10^{-25}$). These data implicate decreased translation in *G-Smo*^{AMPK} tumors.

We next analyzed DEGs in each tumor cluster. 36 different genes were significantly down-regulated in any of the 9 tumor cell clusters of *G-Smo*^{AMPK} tumors and 76 genes significantly up-regulated (Data S1). The DEGs that were decreased in each cluster in *G-Smo*^{AMPK} tumors showed significant overlap (Figures 4A and 4B; $p < 10^{-15}$ by extended hypergeometric test[47]), and the DEGs that were increased also overlapped significantly (p < 0.001 by extended hypergeometric test). AMPK inactivation thus produced changes in gene expression that were common across multiple clusters.

Consistent with pathway enrichment analyses from the comparison of all tumor clusters grouped together, the DEGs that were down-regulated in multiple clusters were associated with translation. We subjected the 14 DEGs down-regulated in 5 or more clusters in *G-Smo*^{AMPK} tumors to PANTHER overrepresentation analysis. The criterion of differentially expressed in 5 or more clusters was used to limit the analysis to genes that were commonly altered in tumor cells in different states. This analysis identified translation as the primary process statistically implicated (corrected $p < 4x10^{-23}$), driven by multiple ribosomal proteins and the translation elongation factor *Eef1b2* (Figure 4B). In contrast

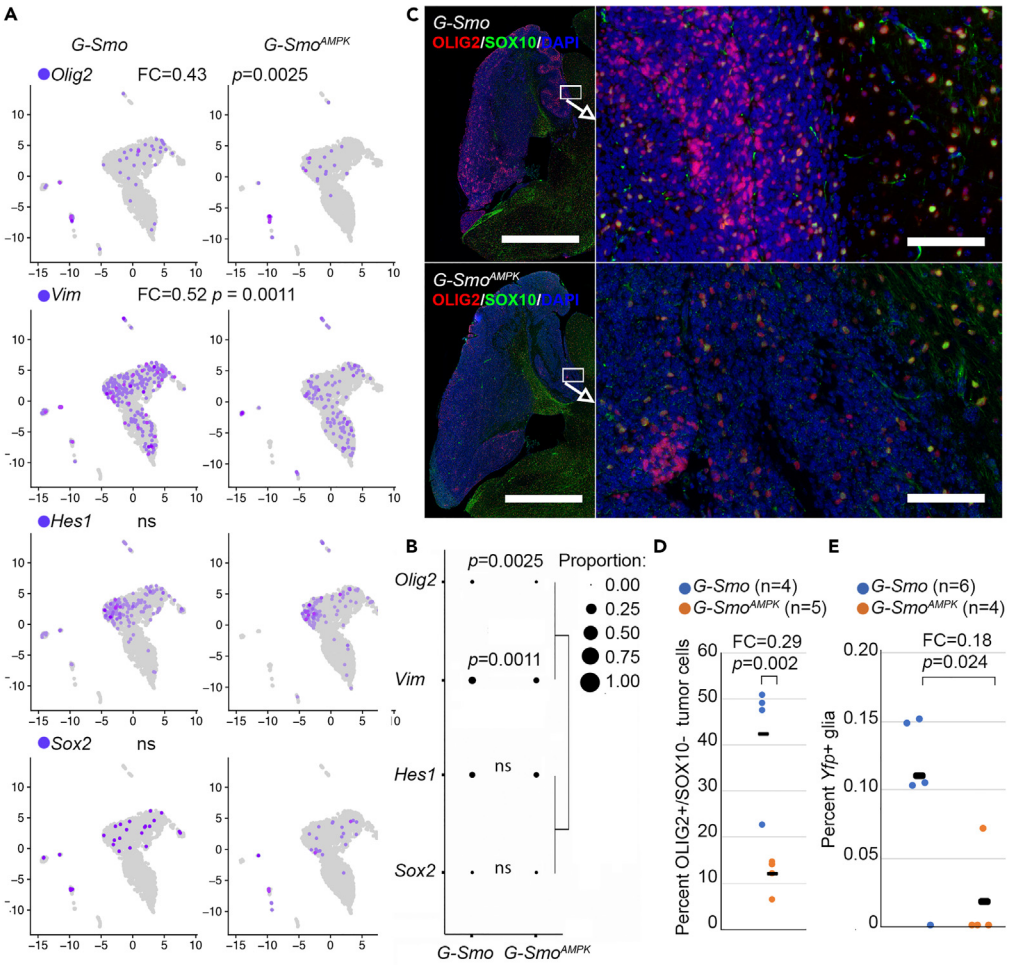

Figure 3. Decreased stem cell populations in *G-Smo*^{AMPK} tumors

(A) Expression of indicated stem cell markers in the indicated genotypes, projected onto the disaggregated UMAPs. *Hes1*, *Sox2*, *Olig2* and *Vim* were significantly lower in *G-Smo*^{AMPK} tumors, while Nes was not significantly different.

(B) Dot plot in which the fractions of cells in each genotype that express the marker are represented by dot size. This panel presents the same data as panel (A), visualized using a different method. Hierarchical clustering show relatively similar variation across genotypes for the group of *Olig2* and *Vim* and for the group of *Sox2* and *Hes1*.

(C) Representative OLIG2/SOX10 IF in sagittal sections of tumors of indicated genotype.

(D) Quantification of OLIG2/SOX10 IF as in (C) in replicate samples of each genotype.

(E) Quantification of *Yfp*+ glial cells in the indicated genotypes. In panels (A), (B), (D) and (E), the p values were determined Student's *t* test. In panel (C), bars = 2 mm in the left panel and 100 μm in the right panel.

to the pattern detected in the down-regulated genes, GO analysis of the 8 genes up-regulated in 5 or more clusters in *G-Smo*^{AMPK} tumors did not identify a statistically implicated process. Thus, while the common process underlying the up-regulation of similar genes in multiple clusters remained cryptic, the pattern of genes recurrently down-regulated in multiple clusters indicated reduced translation.

The mTORC1 pathway is known to regulate translation and ribosomal biogenesis,[48,49] and we speculated that the decreased expression of translation-related and ribosomal genes in *G-Smo*^{AMPK} medulloblastomas might reflect decreased mTORC1 activity in the tumors. In support of this proposed connection to mTORC1 activity, we previously found that the down-regulation of translation-related genes in medulloblastomas treated with palbociclib correlated with decreased mTORC1 signaling.[50] We therefore investigated whether mTORC1 signaling was reduced in in *G-Smo*^{AMPK} tumors.

To quantify mTORC1 activation in tumors, we analyzed the phosphorylation of the mTORC1 substrate 4EBP1 (p4EBP1) using IF, comparing *G-Smo*^{AMPK} and control tumors (Figure 4C). *G-Smo*^{AMPK} tumors showed significantly fewer p4EBP1+ cells (FC = 0.84; p = 0.0002; Student's *t* test) (Figure 4D). Both the recurrent patterns of differential gene expression across clusters and the p4EBP1 studies show reduced mTORC1 activation in *G-Smo*^{AMPK} tumors compared to *G-Smo* control tumors. AMPK is known to inhibit mTORC1,[51–53] and the reduced mTORC1 activity in *G-Smo*^{AMPK} tumors is opposite of the predicted effect of acute AMPK inhibition. While this unexpected suppression of mTORC1

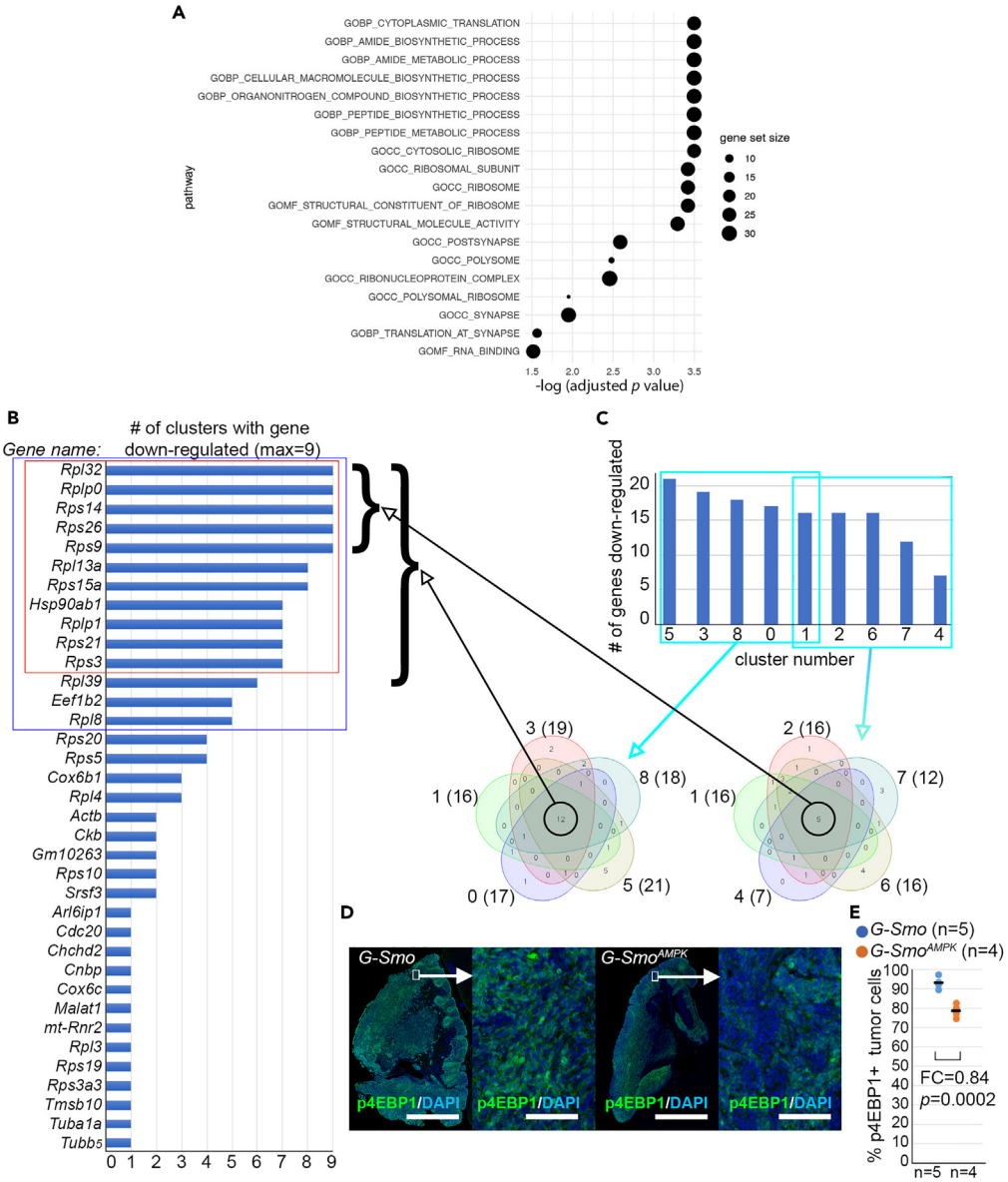

Figure 4. Decreased mTORC1 activity in *G-Smo*^{AMPK} tumors

(A) GSEA showing the pathways significantly enriched in the DEGs in the tumor cells from *G-Smo*^{AMPK} mice versus *G-Smo* controls (B) Genes that are down-regulated in 1 or more clusters, ranked by number of clusters with differential expression. Red box marks the 11 genes down-regulated in 7/9 clusters. Blue box marks the 14 genes down regulated in 5/9 clusters.

(C) Venn diagrams of the genes down-regulated in the 5/9 clusters with the highest number of differentially expressed genes, or in the 5/9 clusters with the fewest differentially expressed genes. Cluster 1 is included in both Venn diagrams as a point of consistency, as depicted in the graph. In each Venn diagram, the cluster number is indicated followed by the number of DEGs for that cluster in parentheses. These Venn diagrams depict sets of 12 or 5 genes down-regulated in all included clusters and brackets show the indicated sets of genes commonly down-regulated genes in the list from (B).

(D) Representative p4EBP1 IF in sagittal sections of tumors of indicated genotype. (E) Quantification of p4EBP1 IF as in (D) in replicate samples of each genotype, compared by Student's *t* test. In panel (D), bars = 2 mm in the low magnification image and 100 μm in the higher magnification image.

activity may result from a homeostatic response to the sustained AMPK inactivation in *G-Smo*^{AMPK} tumors, more information on the timing of the onset of reduced mTORC1 activity will be needed to establish the temporal dynamics of the effect.

Altered glycolytic gene expression in AMP-activated kinase-inactivated medulloblastomas

We previously found that HK2-dependent aerobic glycolysis interacts with AMPK and maintains undifferentiated populations within SHH-driven medulloblastomas. In these prior studies, we conditionally deleted *Hk2* in medulloblastomas by crossing *G-Smo* mice with

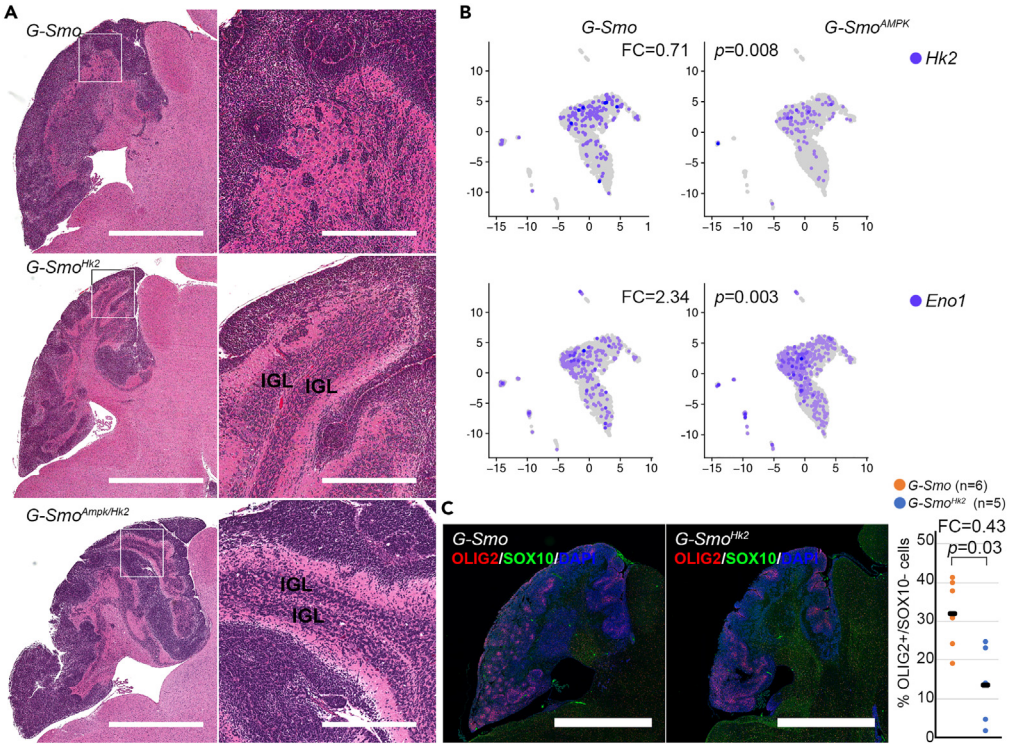

Figure 5. Defining the interaction of AMPK and HK2

(A) Representative H&E sections compare *G-Smo* control tumors to tumors with the deletion of *Hk2* or co-deletion of *Hk2*, *Prkaa1* and *Prkaa2*. Increased differentiation in Hk2-deleted tumors is not rescued by the co-deletion of *Prkaa1* and *Prkaa2*. IGL regions in *G-Smo*^{Hk2} and *G-Smo*^{AMPK} tumors are indicated.

(B) scRNA-seq data showing decreased Hk2 and increased Eno1 in *M-Smo*^{AMPK} tumors.

(C) Representative OLIG2 immunofluorescence, comparing *G-Smo* and Hk2-deleted medulloblastomas, with the quantification of replicate samples. p value determined by Student's *t* test. Bars = 1 mm in the left panel and 25 μm in the right panel (A). Bars = 1 mm in C.

mice that harbor conditional *Hk2* deletion (*Hk2* $^{loxP/loxP}$) to produce the genotype *Gfap-Cre/SmoM2/Hk2* $^{loxP/loxP}$ (*G-Smo*^{Hk2}). We found *G-Smo*^{Hk2} mice developed medulloblastomas with increased differentiation, and that these tumors progressed more slowly, resulting in increased event-free survival of *G-Smo*^{Hk2} mice compared to *G-Smo* mice.[7] *G-Smo*^{Hk2} tumors also showed markedly increased AMPK activation, compared to *G-Smo* tumors.[7] The coincident findings of AMPK activation and increased in differentiation in *Hk2*-deleted tumors suggested a model in which *Hk2* deletion causes AMPK activation and AMPK activation causes increased differentiation. However, our current finding of increased differentiation in *G-Smo*^{AMPK} tumors demonstrates that differentiation does not require AMPK activation, suggesting that the interaction between *Hk2* deletion and AMPK activation may not drive reduced tumor growth in the *G-Smo*^{Hk2} phenotype.

To test directly whether HK2 modulates differentiation through AMPK, we bred mice with medulloblastomas with the deletion of both *Hk2* and *Prkaa1/2*. We crossed *Gfap-Cre/Prkaa1*$^{loxP/loxP}$/*Prkaa2* $^{loxP/loxP}$/*Hk2* $^{loxP/loxP}$ mice with *SmoM2/Prkaa1*$^{loxP/loxP}$/*Prkaa2* $^{loxP/loxP}$/*Hk2* $^{loxP/loxP}$ mice to generate the genotype *Gfap-Cre/SmoM2/Prkaa1*$^{loxP/loxP}$/*Prkaa2* $^{loxP/loxP}$/*Hk2* $^{loxP/loxP}$ (*G-Smo*$^{AMPK/Hk2}$). These *G-Smo*$^{AMPK/Hk2}$ mice developed medulloblastomas with 100% frequency, and the tumors resembled the previously described *G-Smo*^{Hk2} medulloblastomas, marked by regions of differentiation (Figure 5A).[7] These co-deletion studies show that the increased differentiation phenotype caused by *Hk2* deletion does not require AMPK activity, and therefore that AMPK does not operate downstream of HK2-dependent glycolysis to regulate differentiation. In light of these findings, we examined the alternative possibility suggested by AMPK activation in *Hk2*-deleted tumors, that AMPK may operate upstream to induce HK2-dependent aerobic glycolysis.

To determine whether AMPK activity regulates the glycolytic state change that we have previously observed in CGNPs and SHH-driven medulloblastoma,[7] we compared the number of cells expressing each gene in the glycolytic pathway in *G-Smo*^{AMPK} medulloblastomas compared to control tumors. This analysis showed significant differences in the fractions of cells expressing *Hk2* and *Eno1* in AMPK-deleted tumors. *Hk2*+ cells were significantly reduced in *G-Smo*^{AMPK} tumor cells (FC = 0.71; p = 0.008; Student's *t* test) (Figure 5B), consistent with the hypothesis that AMPK activity induces HK2 in SHH-driven medulloblastoma, as seen in prior studies of normal muscle cells.[54] In contrast, cells expressing *Eno1*, which acts at the end of glycolysis, were increased in *G-Smo*^{AMPK} tumors (FC = 2.34; p = 0.003; Student's *t* test) (Figure 5B). AMPK inactivation thus induced specific changes in glycolytic gene expression, predicted to reduce the entry of glucose into glycolysis and to increase the processing of glycolytic intermediates toward pyruvate.

Similar stem cell changes in AMP-activated kinase-inactivated and *Hk2*-deleted medulloblastomas

To determine if alterations in glycolysis may produce specific features of the AMPK-inactivation phenotype, we analyzed OLIG2+ populations in *Hk2*-deleted medulloblastomas. Comparing *G-Smo/Hk2*^{floxed} mice to *G-Smo* controls we found that *Hk2*-deletion was sufficient to reduce the fraction of OLIG2+ tumor cells (FC = 0.43; p = 0.03; Student's *t* test) (Figure 5C). Reduced tumor stem cell populations was thus a common feature of AMPK-inactivated and *Hk2*-deleted medulloblastomas, suggesting that both genes operate in a common pathway to maintain tumor stem cell populations.

DISCUSSION

Medulloblastomas are highly proliferative tumors that configure energy metabolism to support malignant growth through enhanced aerobic glycolysis[7,17] and lipogenesis.[18,55] AMPK is an intracellular energy sensor that coordinates anabolic and catabolic processes with nutrient availability and may crucially regulate tumor metabolism in ways that might be predicted either to support or to inhibit tumor growth. In SHH signaling, AMPK has been shown to interact directly with GLI1 to suppress SHH activity in medulloblastoma.[56,57] In contrast to the anti-tumor effects of AMPK predicted by its interactions with GLI1, however, a prior study of SHH medulloblastoma showed that the deletion of AMPK subunit *Prkaa2* slowed tumor progression in a primary mouse model.[31] Understanding the mechanisms through which AMPK inactivation reduces medulloblastoma growth may allow the design of targeted therapies that exploit the role of AMPK in SHH medulloblastoma and potentially in other cancers.

Our data show that AMPK inactivation slowed medulloblastoma growth and altered tumor cell heterogeneity by disproportionately impacting tumor stem cells. We inactivated AMPK by conditionally deleting both catalytic subunits, *Prkaa1* and *Prkaa2,* in mice carrying *Gfap-Cre* and *SmoM2* alleles, generating *G-Smo*^{AMPK} mice with AMPK inactivation and SHH hyperactivation throughout the brain. In these mice, AMPK-inactivated medulloblastomas formed with 100% penetrance but progressed more slowly than medulloblastomas in controls with SHH hyperactivation but intact AMPK. Like control tumors, AMPK-inactivated tumors comprised medulloblastoma cells with a range of differentiation states. However, AMPK-inactivated medulloblastomas showed a shift in cell populations, with increased differentiated cells compared to controls and specifically reduced populations of OLIG2+ stem cells and malignant glia.

While AMPK inactivation affected different types of tumor cells in different ways, increasing differentiating populations and decreasing tumor stem cells, the effects of gene expression were consistent across multiple cell types. In tumor cells across the differentiation spectrum, AMPK inactivation decreased the expression of multiple genes related to protein translation. This global down-regulation of translation-related genes suggested reduced mTORC1 activity, which was confirmed by the finding of reduced p4EBP1. A decrease in mTORC1 signaling in *G-Smo*^{AMPK} tumors was unexpected, as acute AMPK activation inhibits mTOR.[58,59] We speculate that *G-Smo*^{AMPK} tumor cells reduce mTORC1 in a homeostatic response to AMPK inactivation.

G-Smo^{AMPK} medulloblastomas also showed altered expression of glycolytic genes, with decreased *Hk2* and increased *Eno1*. By impeding the entry of glucose into the glycolysis through HK2 and enhancing the exit of glycolytic intermediates as phosphoenolpyruvate through ENO1, AMPK inactivation reduced the potential for the diversion of glycolytic intermediates for other purposes.

We noted specific changes in the stromal populations in AMPK-inactivated tumors with important implications. Within the stromal populations subject to the deletion of *Prkaa1* and *Prkaa2*, the less mature oligodendrocyte subset was specifically depleted in *G-Smo*^{AMPK} medulloblastomas. While additional studies are needed to confirm these findings from scRNA analysis, oligodendrocytes, such as tumor stem cells, express OLIG2, and their apparently altered differentiation suggests an interaction between AMPK and OLIG2 may crucially modulate OLIG2 function.

Within the stromal populations that were not subject to *Prkaa1* and *Prkaa2* co-deletion, the endothelial cells were significantly increased in *G-Smo*^{AMPK} medulloblastomas. As these cells were not within the GFAP lineage, their increased population cannot be cell autonomous. Increased endothelial populations may indicated changes in tumor vasculature caused by AMPK inactivation in tumor cells, as we have previously seen in glycolysis deficient medulloblastomas.[7] This effect on endothelial cells may thus be another point of similarity between *Hk2*-deleted and AMPK-inactivated medulloblastomas.

By reducing stem cell self-renewal, glial *trans*-differentiation, HK2-dependent aerobic glycolysis and mTORC1 activation, AMPK inactivation altered multiple processes important for tumor progression. Each of these processes has been tested in isolation in previous studies. The maintenance of OLIG2+ stem cell pools has been shown to promote both medulloblastoma progression and recurrence after cytotoxic therapy therapy.[10] HK2-dependent aerobic glycolysis is similarly required for tumor progression.[7] Paracrine signaling between malignant glia and myeloid cells within medulloblastomas also promotes tumor growth.[13] The activation of mTORC1 is similarly essential for tumor growth, and mTORC1 inhibition slows progression.[60] All of these processes are likely to be interrelated, and to contribute to the anti-tumor effect of AMPK inactivation. AMPK inactivation thus sets in motion a complex set of processes that result in the observed shift from multipotent stem cells to more differentiated tumor cells, with the net effect of slowing tumor growth.

To define causal relationships between processes that we found to be altered in AMPK-inactivated tumors, we compared the phenotypes of AMPK-inactivated and *Hk2*-deleted tumors. Both *Hk2* deletion and *Prkaa1/Prkaa2* co-deletion slow tumor growth and extend event-free survival. Importantly, *Hk2* deletion impaired stem cell maintenance and increased differentiation, reproducing the altered cellular heterogeneity of the *Prkaa1/Prkaa2* co-deleted tumors. These genetic data provide evidence for a linear pathway in which AMPK and HK2 both operate in the same direction to maintain undifferentiated, pluripotent populations within medulloblastomas.

The effect of AMPK inactivation on OLIG2+ stem cells identifies a vulnerability that may be exploited therapeutically for clinical benefit. Tumor stem cells are intrinsically resistant to cytotoxic therapy and drive recurrence. Ways to target these stem cells are urgently needed. Our

data show that chronic blockade of AMPK activity disproportionately affects these stem cells, suggesting a way to target these otherwise resistant populations. Follow up studies are needed to test pharmacologic AMPK inhibition in combination with current, cytotoxic therapy. As genetic deletion studies demonstrate that AMPK inactivation can suppress tumor growth, and AMPK deletion in model organisms does not have clear deleterious effects,[29] AMPK inhibition may emerge as an important new avenue for cancer therapy.

Limitations of the study

We demonstrate that AMPK inactivation slows tumor progression in SHH medulloblastoma, reduces mTORC1 activity and depletes stem cell populations that express OLIG2. However, the precise mechanisms for the down-regulation of mTORC1 and the disproportionate impact on tumor stem cells are not clear. Additionally, we did not consider sex-specific responses in the study. Additional studies are required to investigate how sustained inactivation of AMPK, which is known to phosphorylate mTORC1, results in net mTORC1 inhibition in tumors *in vivo*, how AMPK contributes to the maintenance of the stem cell phenotype, and whether there are sex-specific differences in stem cell metabolism. Our scRNA-seq studies identified a large number of differentially expressed genes, and we limited our additional validation studies to a subset of these genes selected to confirm biologically relevant trends in the data. The statistical methods applied to the scRNA-seq data require that the assumptions of the statistical models are satisfied, and these assumptions are difficult to evaluate on the limited set of replicates. For this reason, we have limited our conclusions about changes in cellular diversity induced by AMPK activation to phenotypes that we validated by quantitative studies of protein expression, specifically changes in differentiation, proliferation, OLIG2 expression and mTORC1 activation.

STAR★METHODS

Detailed methods are provided in the online version of this paper and include the following:

- KEY RESOURCES TABLE
- RESOURCE AVAILABILITY
  - Lead contact
  - Materials availability
  - Data and code availability
- EXPERIMENTAL MODEL AND STUDY PARTICIPANT DETAILS
  - Mice
- METHOD DETAILS
  - Histology and immunofluorescence (IF)
  - Tissue preparation for drop-seq
- QUANTIFICATION AND STATISTICAL ANALYSIS
  - Processing of scRNA-seq data
  - Harmony analysis
  - scRNA-seq data normalization, clustering, differential gene expression, and visualization
  - Cell-type identification
  - Statistical analysis of IF data

SUPPLEMENTAL INFORMATION

Supplemental information can be found online at https://doi.org/10.1016/j.isci.2023.108443.

ACKNOWLEDGMENTS

We thank the UNC CGBID Histology Core, supported by P30 DK 034987 and the UNC Tissue Pathology Laboratory Core supported by NCI CA016086. T.D. was supported by NINDS (F31 NS120459). T.R.G. was supported by NINDS (R01NS088219, R01NS102627, R01NS106227)and by the UNC Department of Neurology Research Fund, and by a TTSA grant from the NCTRACS Institute, which is supported by the National Center for Advancing Translational Sciences (NCATS), National Institutes of Health, through Grant Award Number UL1TR002489.

AUTHOR CONTRIBUTIONS

D.S.M., T.D., J.B., B.D., A.T., and T.R.G. wrote the article. D.S.M., T.D., E.C., and H.L. conducted the experiments and analyzed the data.

DECLARATION OF INTERESTS

The authors declare no competing interests. Ethan Castellino is currently a student at Duke University.

INCLUSION AND DIVERSITY

One or more of the authors of this paper self-identifies as an underrepresented ethnic minority in their field of research or within their geographical location. One or more of the authors of this paper self-identifies as a gender minority in their field of research. One or more

of the authors of this paper received support from a program designed to increase minority representation in their field of research. We worked to ensure sex balance in the selection of non-human subjects.

Received: November 21, 2022
Revised: March 28, 2023
Accepted: November 8, 2023
Published: November 14, 2023

REFERENCES

1. Northcott, P.A., Shih, D.J.H., Peacock, J., Garzia, L., Morrissy, A.S., Zichner, T., Stütz, A.M., Korshunov, A., Reimand, J., Schumacher, S.E., et al. (2012). Subgroup-specific structural variation across 1,000 medulloblastoma genomes. Nature *488*, 49–56.
2. Kool, M., Korshunov, A., Remke, M., Jones, D.T.W., Schlanstein, M., Northcott, P.A., Cho, Y.J., Koster, J., Schouten-van Meeteren, A., van Vuurden, D., et al. (2012). Molecular subgroups of medulloblastoma: an international meta-analysis of transcriptome, genetic aberrations, and clinical data of WNT, SHH, Group 3, and Group 4 medulloblastomas. Acta Neuropathol. *123*, 473–484.
3. Northcott, P.A., Korshunov, A., Witt, H., Hielscher, T., Eberhart, C.G., Mack, S., Bouffet, E., Clifford, S.C., Hawkins, C.E., French, P., et al. (2011). Medulloblastoma comprises four distinct molecular variants. J. Clin. Oncol. *29*, 1408–1414.
4. Cavalli, F.M.G., Remke, M., Rampasek, L., Peacock, J., Shih, D.J.H., Luu, B., Garzia, L., Torchia, J., Nor, C., Morrissy, A.S., et al. (2017). Intertumoral Heterogeneity within Medulloblastoma Subgroups. Cancer Cell *31*, 737–754.e6.
5. Riemondy, K.A., Venkataraman, S., Willard, N., Nellan, A., Sanford, B., Griesinger, A.M., Amani, V., Mitra, S., Hankinson, T.C., Handler, M.H., et al. (2021). Neoplastic and Immune single cell transcriptomics define subgroup-specific intra-tumoral heterogeneity of childhood medulloblastoma. Neuro Oncol. *24*, 273–286.
6. Hovestadt, V., Smith, K.S., Bihannic, L., Filbin, M.G., Shaw, M.L., Baumgartner, A., DeWitt, J.C., Groves, A., Mayr, L., Weisman, H.R., et al. (2019). Resolving medulloblastoma cellular architecture by single-cell genomics. Nature *572*, 74–79.
7. Gershon, T.R., Crowther, A.J., Tikunov, A., Garcia, I., Annis, R., Yuan, H., Miller, C.R., Macdonald, J., Olson, J., and Deshmukh, M. (2013). Hexokinase-2-mediated aerobic glycolysis is integral to cerebellar neurogenesis and pathogenesis of medulloblastoma. Cancer Metab. *1*, 2.
8. Oliver, T.G., Read, T.A., Kessler, J.D., Mehmeti, A., Wells, J.F., Huynh, T.T.T., Lin, S.M., and Wechsler-Reya, R.J. (2005). Loss of patched and disruption of granule cell development in a pre-neoplastic stage of medulloblastoma. Development *132*, 2425–2439.
9. Hallahan, A.R., Pritchard, J.I., Hansen, S., Benson, M., Stoeck, J., Hatton, B.A., Russell, T.L., Ellenbogen, R.G., Bernstein, I.D., Beachy, P.A., and Olson, J.M. (2004). The SmoA1 mouse model reveals that notch signaling is critical for the growth and survival of sonic hedgehog-induced medulloblastomas. Cancer Res. *64*, 7794–7800.
10. Zhang, L., He, X., Liu, X., Zhang, F., Huang, L.F., Potter, A.S., Xu, L., Zhou, W., Zheng, T., Luo, Z., et al. (2019). Single-Cell Transcriptomics in Medulloblastoma Reveals Tumor-Initiating Progenitors and Oncogenic Cascades during Tumorigenesis and Relapse. Cancer Cell *36*, 302–318.e7.
11. Ocasio, J.K., Babcock, B., Malawsky, D., Weir, S.J., Loo, L., Simon, J.M., Zylka, M.J., Hwang, D., Dismuke, T., Sokolsky, M., et al. (2019). scRNA-seq in medulloblastoma shows cellular heterogeneity and lineage expansion support resistance to SHH inhibitor therapy. Nat. Commun. *10*, 5829.
12. Vladoiu, M.C., El-Hamamy, I., Donovan, L.K., Farooq, H., Holgado, B.L., Sundaravadanam, Y., Ramaswamy, V., Hendrikse, L.D., Kumar, S., Mack, S.C., et al. (2019). Childhood cerebellar tumours mirror conserved fetal transcriptional programs. Nature *572*, 67–73.
13. Yao, M., Ventura, P.B., Jiang, Y., Rodriguez, F.J., Wang, L., Perry, J.S.A., Yang, Y., Wahl, K., Crittenden, R.B., Bennett, M.L., et al. (2020). Astrocytic trans-Differentiation Completes a Multicellular Paracrine Feedback Loop Required for Medulloblastoma Tumor Growth. Cell *180*, 502–520.e19.
14. Hardie, D.G. (2003). Minireview: The AMP-Activated Protein Kinase Cascade: The Key Sensor of Cellular Energy Status. Endocrinology *144*, 5179–5183.
15. Hardie, D.G., Ross, F.A., and Hawley, S.A. (2012). AMP-Activated Protein Kinase: A Target for Drugs both Ancient and Modern. Chem. Biol. *19*, 1222–1236.
16. Tech, K., Deshmukh, M., and Gershon, T.R. (2015). Adaptations of energy metabolism during cerebellar neurogenesis are co-opted in medulloblastoma. Cancer Lett. *356*, 268–272.
17. Tech, K., Tikunov, A.P., Farooq, H., Morrissy, A.S., Meidinger, J., Fish, T., Green, S.C., Liu, H., Li, Y., Mungall, A.J., et al. (2017). Pyruvate Kinase Inhibits Proliferation during Postnatal Cerebellar Neurogenesis and Suppresses Medulloblastoma Formation. Cancer Res. *77*, 3217–3230.
18. Bhatia, B., Hsieh, M., Kenney, A.M., and Nahlé, Z. (2011). Mitogenic Sonic hedgehog signaling drives E2F1-dependent lipogenesis in progenitor cells and medulloblastoma. Oncogene *30*, 410–422.
19. Eyrich, N.W., Potts, C.R., Robinson, M.H., Maximov, V., and Kenney, A.M. (2019). Reactive Oxygen Species Signaling Promotes Hypoxia-Inducible Factor 1alpha Stabilization in Sonic Hedgehog-Driven Cerebellar Progenitor Cell Proliferation. Mol. Cell Biol. *39*. e00268–18.
20. Malhotra, A., Dey, A., Prasad, N., and Kenney, A.M. (2016). Sonic Hedgehog Signaling Drives Mitochondrial Fragmentation by Suppressing Mitofusins in Cerebellar Granule Neuron Precursors and Medulloblastoma. Mol. Cancer Res. *14*, 114–124.
21. Zeng, Q., Chen, J., Li, Y., Werle, K.D., Zhao, R.X., Quan, C.S., Wang, Y.S., Zhai, Y.X., Wang, J.W., Youssef, M., et al. (2017). LKB1 inhibits HPV-associated cancer progression by targeting cellular metabolism. Oncogene *36*, 1245–1255.
22. Faubert, B., Vincent, E.E., Griss, T., Samborska, B., Izreig, S., Svensson, R.U., Mamer, O.A., Avizonis, D., Shackelford, D.B., Shaw, R.J., and Jones, R.G. (2014). Loss of the tumor suppressor LKB1 promotes metabolic reprogramming of cancer cells via HIF-1alpha. Proc. Natl. Acad. Sci. USA *111*, 2554–2559.
23. Shackelford, D.B., Abt, E., Gerken, L., Vasquez, D.S., Seki, A., Leblanc, M., Wei, L., Fishbein, M.C., Czernin, J., Mischel, P.S., and Shaw, R.J. (2013). LKB1 inactivation dictates therapeutic response of non-small cell lung cancer to the metabolism drug phenformin. Cancer Cell *23*, 143–158.
24. Eichner, L.J., Brun, S.N., Herzig, S., Young, N.P., Curtis, S.D., Shackelford, D.B., Shokhirev, M.N., Leblanc, M., Vera, L.I., Hutchins, A., et al. (2019). Genetic Analysis Reveals AMPK Is Required to Support Tumor Growth in Murine Kras-Dependent Lung Cancer Models. Cell Metab. *29*, 285–302.e7.
25. Muraleedharan, R., and Dasgupta, B. (2022). AMPK in the brain: its roles in glucose and neural metabolism. FEBS J. *289*, 2247–2262.
26. Muraleedharan, R., Gawali, M.V., Tiwari, D., Sukumaran, A., Oatman, N., Anderson, J., Nardini, D., Bhuiyan, M.A.N., Tkáč, I., Ward, A.L., et al. (2020). AMPK-Regulated Astrocytic Lactate Shuttle Plays a Non-Cell-Autonomous Role in Neuronal Survival. Cell Rep. *32*, 108092.
27. Herzig, S., and Shaw, R.J. (2018). AMPK: guardian of metabolism and mitochondrial homeostasis. Nat. Rev. Mol. Cell Biol. *19*, 121–135.
28. Chhipa, R.R., Fan, Q., Anderson, J., Muraleedharan, R., Huang, Y., Ciraolo, G., Chen, X., Waclaw, R., Chow, L.M., Khuchua, Z., et al. (2018). AMP kinase promotes glioblastoma bioenergetics and tumour growth. Nat. Cell Biol. *20*, 823–835.
29. Williams, T., Courchet, J., Viollet, B., Brenman, J.E., and Polleux, F. (2011). AMP-activated protein kinase (AMPK) activity is not required for neuronal development but regulates axogenesis during metabolic stress. Proc. Natl. Acad. Sci. USA *108*, 5849–5854.
30. Dzamko, N., van Denderen, B.J.W., Hevener, A.L., Jørgensen, S.B., Honeyman, J., Galic, S., Chen, Z.P., Watt, M.J., Campbell, D.J., Steinberg, G.R., and Kemp, B.E. (2010). AMPK beta1 deletion reduces appetite, preventing obesity and hepatic insulin resistance. J. Biol. Chem. *285*, 115–122.

31. Zhang, H., Kuick, R., Park, S.S., Peabody, C., Yoon, J., Fernández, E.C., Wang, J., Thomas, D., Viollet, B., Inoki, K., et al. (2018). Loss of AMPKalpha2 Impairs Hedgehog-Driven Medulloblastoma Tumorigenesis. Int. J. Mol. Sci. *19*, 3287.
32. D'Amico, D., Antonucci, L., Di Magno, L., Coni, S., Sdruscia, G., Macone, A., Miele, E., Infante, P., Di Marcotullio, L., De Smaele, E., et al. (2015). Non-canonical Hedgehog/AMPK-Mediated Control of Polyamine Metabolism Supports Neuronal and Medulloblastoma Cell Growth. Dev. Cell *35*, 21–35.
33. Kool, M., Jones, D.T., Jager, N., Northcott, P.A., Pugh, T.J., Hovestadt, V., Piro, R.M., Esparza, L.A., Markant, S.L., Remke, M., et al. (2014). Genome sequencing of SHH medulloblastoma predicts genotype-related response to smoothened inhibition. Cancer Cell *25*, 393–405.
34. Mao, J., Ligon, K.L., Rakhlin, E.Y., Thayer, S.P., Bronson, R.T., Rowitch, D., and McMahon, A.P. (2006). A novel somatic mouse model to survey tumorigenic potential applied to the Hedgehog pathway. Cancer Res. *66*, 10171–10178.
35. Schüller, U., Heine, V.M., Mao, J., Kho, A.T., Dillon, A.K., Han, Y.-G., Huillard, E., Sun, T., Ligon, A.H., Qian, Y., et al. (2008). Acquisition of Granule Neuron Precursor Identity Is a Critical Determinant of Progenitor Cell Competence to Form Shh-Induced Medulloblastoma. Cancer Cell *14*, 123–134.
36. Malawsky, D.S., Weir, S., Ocasio, J., Babcock, B., Dismuke, T., Wilhelmsen, K., and Gershon, T.R. (2020). Cryptic developmental events determine medulloblastoma radiosensitivity and cellular heterogeneity without altering transcriptomic profile. Commun. Biol. *4*, 616.
37. Malawsky, D.S., Weir, S.J., Ocasio, J.K., Babcock, B., Dismuke, T., Cleveland, A.H., Donson, A.M., Vibhakar, R., Wilhelmsen, K., and Gershon, T.R. (2021). Cryptic developmental events determine medulloblastoma radiosensitivity and cellular heterogeneity without altering transcriptomic profile. Commun. Biol. *4*, 616.
38. Swiderska-Syn, M., Mir-Pedrol, J., Oles, A., Schleuger, O., Salvador, A.D., Greiner, S.M., Seward, C., Yang, F., Babcock, B.R., Shen, C., et al. (2022). Noncanonical activation of GLI signaling in SOX2(+) cells drives medulloblastoma relapse. Sci. Adv. *8*, eabj9138.
39. Lim, C., Dismuke, T., Malawsky, D., Ramsey, J.D., Hwang, D., Godfrey, V.L., Kabanov, A.V., Gershon, T.R., and Sokolsky-Papkov, M. (2022). Enhancing CDK4/6 inhibitor therapy for medulloblastoma using nanoparticle delivery and scRNA-seq-guided combination with sapanisertib. Sci. Adv. *8*, eabl5838.
40. Loo, L., Simon, J.M., Xing, L., McCoy, E.S., Niehaus, J.K., Guo, J., Anton, E.S., and Zylka, M.J. (2019). Single-cell transcriptomic analysis of mouse neocortical development. Nat. Commun. *10*, 134.
41. Luecken, M.D., and Theis, F.J. (2019). Current best practices in single-cell RNA-seq analysis: a tutorial. Mol. Syst. Biol. *15*, e8746.
42. Li, S., Qiu, F., Xu, A., Price, S.M., and Xiang, M. (2004). Barhl1 regulates migration and survival of cerebellar granule cells by controlling expression of the neurotrophin-3 gene. J. Neurosci. *24*, 3104–3114.
43. Miyata, T., Maeda, T., and Lee, J.E. (1999). NeuroD is required for differentiation of the granule cells in the cerebellum and hippocampus. Genes Dev. *13*, 1647–1652.
44. Malawsky, D., and Gershon, T.R. (2023). scRNA-seq for Microcephaly Research [IV]: Dirichlet Regression for Single-Cell Population Differences. Methods Mol. Biol. *2583*, 123–125.
45. Hambardzumyan, D., Becher, O.J., Rosenblum, M.K., Pandolfi, P.P., Manova-Todorova, K., and Holland, E.C. (2008). PI3K pathway regulates survival of cancer stem cells residing in the perivascular niche following radiation in medulloblastoma in vivo. Genes Dev. *22*, 436–448.
46. Crowther, A.J., Ocasio, J.K., Fang, F., Meidinger, J., Wu, J., Deal, A.M., Chang, S.X., Yuan, H., Schmid, R., Davis, I., and Gershon, T.R. (2016). Radiation Sensitivity in a Preclinical Mouse Model of Medulloblastoma Relies on the Function of the Intrinsic Apoptotic Pathway. Cancer Res. *76*, 3211–3223.
47. Kalinka, A. (2013). The probability of drawing intersections: extending the hypergeometric distribution. Preprint at arXiv. https://arxiv.org/abs/1305.0717.
48. Morita, M., Gravel, S.P., Chénard, V., Sikström, K., Zheng, L., Alain, T., Gandin, V., Avizonis, D., Arguello, M., Zakaria, C., et al. (2013). mTORC1 controls mitochondrial activity and biogenesis through 4E-BP-dependent translational regulation. Cell Metab. *18*, 698–711.
49. Thoreen, C.C., Chantranupong, L., Keys, H.R., Wang, T., Gray, N.S., and Sabatini, D.M. (2012). A unifying model for mTORC1-mediated regulation of mRNA translation. Nature *485*, 109–113.
50. Lim, C., Dismuke, T., Malawsky, D., Ramsey, J.D., Hwang, D., Godfrey, V.L., Kabanov, A.V., Gershon, T.R., and Sokolsky-Papkov, M. (2021). Enhancing CDK4/6 inhibitor therapy for medulloblastoma using nanoparticle delivery and scRNA-seq-guided combination with sapanisertib. Sci. Adv. *8*, eabl5838.
51. Gwinn, D.M., Shackelford, D.B., Egan, D.F., Mihaylova, M.M., Mery, A., Vasquez, D.S., Turk, B.E., and Shaw, R.J. (2008). AMPK phosphorylation of raptor mediates a metabolic checkpoint. Mol. Cell *30*, 214–226.
52. Corradetti, M.N., Inoki, K., Bardeesy, N., DePinho, R.A., and Guan, K.L. (2004). Regulation of the TSC pathway by LKB1: evidence of a molecular link between tuberous sclerosis complex and Peutz-Jeghers syndrome. Genes Dev. *18*, 1533–1538.
53. Inoki, K., Zhu, T., and Guan, K.L. (2003). TSC2 mediates cellular energy response to control cell growth and survival. Cell *115*, 577–590.
54. Stoppani, J., Hildebrandt, A.L., Sakamoto, K., Cameron-Smith, D., Goodyear, L.J., and Neufer, P.D. (2002). AMP-activated protein kinase activates transcription of the UCP3 and HKII genes in rat skeletal muscle. Am. J. Physiol. Endocrinol. Metab. *283*, E1239–E1248.
55. Bhatia, B., Potts, C.R., Guldal, C., Choi, S., Korshunov, A., Pfister, S., Kenney, A.M., and Nahlé, Z.A. (2012). Hedgehog-mediated regulation of PPARgamma controls metabolic patterns in neural precursors and shh-driven medulloblastoma. Acta Neuropathol. *123*, 587–600.
56. Li, Y.H., Luo, J., Mosley, Y.Y.C., Hedrick, V.E., Paul, L.N., Chang, J., Zhang, G., Wang, Y.K., Banko, M.R., Brunet, A., et al. (2015). AMP-Activated Protein Kinase Directly Phosphorylates and Destabilizes Hedgehog Pathway Transcription Factor GLI1 in Medulloblastoma. Cell Rep. *12*, 599–609.
57. Zhang, R., Huang, S.Y., Ka-Wai Li, K., Li, Y.H., Hsu, W.H., Zhang, G.J., Chang, C.J., and Yang, J.Y. (2017). Dual degradation signals destruct GLI1: AMPK inhibits GLI1 through beta-TrCP-mediated proteasome degradation. Oncotarget *8*, 49869–49881.
58. Kimura, N., Tokunaga, C., Dalal, S., Richardson, C., Yoshino, K.i., Hara, K., Kemp, B.E., Witters, L.A., Mimura, O., and Yonezawa, K. (2003). A possible linkage between AMP-activated protein kinase (AMPK) and mammalian target of rapamycin (mTOR) signalling pathway. Gene Cell. *8*, 65–79.
59. Bolster, D.R., Crozier, S.J., Kimball, S.R., and Jefferson, L.S. (2002). AMP-activated protein kinase suppresses protein synthesis in rat skeletal muscle through down-regulated mammalian target of rapamycin (mTOR) signaling. J. Biol. Chem. *277*, 23977–23980.
60. Wu, C.C., Hou, S., Orr, B.A., Kuo, B.R., Youn, Y.H., Ong, T., Roth, F., Eberhart, C.G., Robinson, G.W., Solecki, D.J., et al. (2017). mTORC1-Mediated Inhibition of 4EBP1 Is Essential for Hedgehog Signaling-Driven Translation and Medulloblastoma. Dev. Cell *43*, 673–688.e5.
61. Korsunsky, I., Millard, N., Fan, J., Slowikowski, K., Zhang, F., Wei, K., Baglaenko, Y., Brenner, M., Loh, P.R., and Raychaudhuri, S. (2019). Fast, sensitive and accurate integration of single-cell data with Harmony. Nat. Methods *16*, 1289–1296.
62. Ocasio, J.K., Bates, R.D.P., Rapp, C.D., and Gershon, T.R. (2019). GSK-3 modulates SHH-driven proliferation in postnatal cerebellar neurogenesis and medulloblastoma. Development *146*, dev177550.
63. Lang, P.Y., Nanjangud, G.J., Sokolsky-Papkov, M., Shaw, C., Hwang, D., Parker, J.S., Kabanov, A.V., and Gershon, T.R. (2016). ATR maintains chromosomal integrity during postnatal cerebellar neurogenesis and is required for medulloblastoma formation. Development *143*, 4038–4052.
64. Macosko, E.Z., Basu, A., Satija, R., Nemesh, J., Shekhar, K., Goldman, M., Tirosh, I., Bialas, A.R., Kamitaki, N., Martersteck, E.M., et al. (2015). Highly Parallel Genome-wide Expression Profiling of Individual Cells Using Nanoliter Droplets. Cell *161*, 1202–1214.
65. Butler, A., Hoffman, P., Smibert, P., Papalexi, E., and Satija, R. (2018). Integrating single-cell transcriptomic data across different conditions, technologies, and species. Nat. Biotechnol. *36*, 411–420.
66. La Manno, G., Siletti, K., Furlan, A., Gyllborg, D., Vinsland, E., Mossi Albiach, A., Mattsson Langseth, C., Khven, I., Lederer, A.R., Dratva, L.M., et al. (2021). Molecular architecture of the developing mouse brain. Nature *596*, 92–96.

STAR★METHODS

KEY RESOURCES TABLE

REAGENT or RESOURCE	SOURCE	IDENTIFIER
Antibodies		
OLIG2	Cell Marque	Cat.# 387R-14
Sox10	Cell Signaling Technology	Cat.# 7833S
PRB	Cell Signaling Technology	Cat.# 8957
NeuN	Millipore	Cat.# MAB377; RRID: AB_2298772
Ki67	Cell Signaling Technology	Cat.# 12202S
NeuroD1	Abcam	Cat.# ab213725; RRID: AB_2801303
p4EBP1	Cell Signaling Technology	Cat.# 2855
Critical commercial assays		
Papain Dissociation System	Worthington Biochemical	Cat.# LK003150
Barcoded Seq B Drop-seq beads	ChemGenes	Cat.# Macosko-2011-10(V+)
PDMS device	FlowJEM	Request: "Drop-Seq Device with Aquapel Coating"
Deposited data		
scRNA-seq raw and analyzed data	This paper	GEO: GSE150579
scRNA-seq raw and analyzed data	This paper	GEO: GSE190297
Mouse: GFAP-Cre: FVB-Tg(GFAP-cre)25Mes/J	The Jackson Laboratory	RRID:IMSR_JAX:004600
Mouse: Prkaa1^{loxP}: Prkar1a$^{tm1.2Lsk}$/J	The Jackson Laboratory	RRID:IMSR_JAX:036801
Mouse: Prkaa2^{loxP}: Prkaa2$^{tm1.1Sjm}$/J	The Jackson Laboratory	RRID:IMSR_JAX:014142
Mouse: SmoM2: Gt(ROSA)26Sor$^{tm1(Smo/EYFP)Amc}$/J	The Jackson Laboratory	RRID:IMSR_JAX:005130
Mouse: C57BL/6:	The Jackson Laboratory	RRID:IMSR_JAX:000664
Software and algorithms		
Seurat R package version 3.1.1	Satija Lab	https://cran.r-project.org/src/contrib/Archive/Seurat/Seurat_3.1.1.tar.gz
Harmony algorithm	Korsunsky et al.[61]	https://github.com/immunogenomics/harmony
Tissue Studio 4.4.2	Definiens	Build 60765 x64

RESOURCE AVAILABILITY

Lead contact

Further information and and requests for resources and reagents should be directed to and will be fulfilled by the lead contact: Timothy R. Gershon, MD, PhD, timothy.gershon@emory.edu.

Materials availability

Identification information for the *GFAP-Cre* (JAX:004600) *Prkaa1*^{loxP} (JAX:036801), *Prkaa2*^{loxP} (JAX:014142), *SmoM2* (JAX:005130) and C57BL/6 (JAX:000664) mouse lines are available from Jackson Labs.

Data and code availability

- The scRNA-seq data were deposited in the Gene Expression Omnibus (GEO) database and are publicly available at the time of publication. Accession codes are listed in the key resources table. Microscopy data reported in the paper will be shared by the lead contact upon request.
- This paper did not use or create original code. The scRNA-seq analysis was performed using the publicly available Seurat R package version 3.1.1.
- Any additional information required to reanalyze the data reported in this paper will be made available by the lead contact upon request.

EXPERIMENTAL MODEL AND STUDY PARTICIPANT DETAILS

Mice

We crossed *SmoM2* mice (Jackson Labs, stock # 005130) with *GFAP-Cre* mice (Jackson Labs, stock # 004600), to generate *GFAP-Cre/SmoM2* (*G-Smo*) mice. We crossed *Prkaa1*$^{loxP/loxP}$/*Prkaa2* $^{loxP/loxP}$ mice that harbor *loxP* sites flanking the coding regions of *Prkaa1 and Prkaa2*[29] with GFAP-Cre mice to generate *Gfap-Cre/Prkaa1*$^{loxP/loxP}$/*Prkaa2* $^{loxP/loxP}$ (*G-Cre*^{AMPK}) mice. These mice have been previously published and the effective depletion of PRKAA1 and PRKAA2 proteins in the brains of these mice has been demonstrated.[29] We then crossed *G-Cre*^{AMPK} mice with *SmoM2* mice generate *G-Smo*^{AMPK} mice with *Prkaa1/2*-deleted medulloblastomas. All mice were of species Mus musculus and crossed into the C57BL/6 background through at least five generations. All animal studies were carried out with the approval of the University of North Carolina Institutional Animal Care and Use Committee under protocols (19–098 and 21-011). Male and female animals were randomly selected for each experimental condition.

All mice were immunocompetent and not known to have any confounding health conditions. No animals were previously used in other experiments. All animals were drug naive and no animals were treated with any agents. All mice were housed and maintained by the University of North Carolina Department of Comparative Medicine under standard, humane husbandry conditions. No cell lines were used.

METHOD DETAILS

Histology and immunofluorescence (IF)

Mouse brains were processed, immunostained and quantitatively analyzed as previously described.[11,46,62] Briefly, slides were de-paraffinized and stained in an automated processor. Primary antibodies used were: OLIG2 diluted 1:100 (Cell Marque, # 387R-14), SOX10 diluted 1:200 (Cell Signaling Technology, #7833S). Stained images were counterstained with DAPI, digitally imaged using an Aperio Scan Scope XT (Aperio) and imported to Definiens Architect XD 2.7 Build 60765 x64 for analysis with Tissue Studio version 4.4.2.

Tissue preparation for drop-seq

Data from *G-Smo* and *G-Smo*^{AMPK} tumors were obtained by Drop-seq in separate batches, using the same methods as described below. The *G-Smo* data was previously published[37] and made publicly available, while the *G-Smo*^{AMPK} data were newly obtained for this study. In both batches, mice were euthanized by decapitation under isoflurane anesthesia. The brain was divided along the sagittal midline and one-half was processed for histology and a sample of tumor was dissected from the other half and processed for Drop-seq analysis. This sample was dissociated using the Papain Dissociation System (Worthington Biochemical) following the protocol used in previous studies.[11,63] Briefly, tumor samples were incubated in papain at 37°C for 15 min, then triturated and the suspended cells were spun through a density gradient of ovomucoid inhibitor.

We resuspended pelleted cells in 1 mL HBSS with 6 g/L glucose and diluted in PBS-BSA solution to a concentration of 95–110 cells/μL. Barcoded Seq B Drop-seq beads (ChemGenes) were diluted in Drop-seq lysis buffer to a concentration between 95 and 110 beads/μL. Tumor cells were co-encapsulated with barcoded beads using FlowJEM brand PDMS devices as previously described.[11] All cells were processed within 1 h of tissue dissociation. Droplet breakage and library preparation steps followed Drop-seq protocol V3.1.[64] After PCR, amplified cDNA was subjected to Ampure XP cleanup at 0.6x and 1x ratios to eliminate residual PCR primers and debris. If PCR failed to generate adequate cDNA, the PCR was repeated with the 3rd round increased from 11 to 13 cycles.

For quality control (QC) purposes, library pools consisting of the tagmented cDNA from 2,000 beads/run were prepared and sequenced to low depth (~2.5M reads/2K beads). We used the resulting data to assess library efficiency, including total read losses to PolyA regions, nonsense barcodes and adapter sequences as well as the quality and number of the transcriptomes captured. Passable runs contained 40–60% of reads associated with the top 80–100 barcodes found in 2,000 beads. Drop-seq runs passing QC were then prepared for high-depth sequencing on an Illumina Novaseq S2 flow cell.

QUANTIFICATION AND STATISTICAL ANALYSIS

Processing of scRNA-seq data

Data analysis was performed using the Seurat R package version 3.1.1.[65] Data were subjected to several filtering steps. First, only genes that were detected in at least 30 cells were considered, to prevent misaligned reads appearing as rare transcripts in the data. Cells were then filtered using specific QC criteria to limit the analysis to cells with transcriptomes that were well-characterized and not apoptotic. 4,930 out of 6,743 putative *G-Smo*^{AMPK} cells, and 8699 out of 16489 *G-Smo* cells met criteria and were included in the analysis.

We noted that *G-Smo* cells were sequenced at a greater depth than *G-Smo*^{AMPK} cells which can introduce unwanted batch effects into the analysis. Consistent with best practices,[41] we down-sampled the *G-Smo* cells to 46.5% of their original depth so as to achieve similar sequencing depth between *G-Smo* and *G-Smo*^{AMPK} cells prior to further filtering.

We filtered out putative cells with fewer than 500 detected RNA molecules (nCount) or 200 different genes (nFeature), as likely to represent ambient RNA. We filtered out putative cells with greater than 4 standard deviations above the median nCount or nFeature as likely to be doublets, improperly merged barcodes, or sequencing artifacts. We also filtered out putative cells with more than 10% mitochondrial transcripts which we suspected to be dying cells.

Harmony analysis

To merge the previously published *G-Smo* control tumor data with the *G-Smo*^{AMPK} tumor dataset, we used the Harmony algorithm.[65] First, data from both tumor types were analyzed in single SCTransform normalization and PCA steps. The Harmony algorithm then used the cells' PCA coordinates and dataset identity to calculate new coordinates for each cell, to minimize dataset dependence when applying clustering to the cells. This algorithm produced a dimensional reduction that was used as a PCA for the following steps of the analysis.

scRNA-seq data normalization, clustering, differential gene expression, and visualization

We normalized the data using the SCTransform as implemented in Seurat, then selected the top 3,000 most highly variable genes. We performed PCA on these highly variable genes using the RunPCA function. The number of PCs to be used in downstream analysis was chosen based on the elbow plot as implemented by Seurat. We then used the FindNeighbors and FindClusters functions to identify cell clusters in the data.

To identify differential genes between clusters of cells, we used Wilcoxon rank-sum test to compare gene expression of cells within the cluster of interest to all cells outside that cluster as implemented by the FindMarkers function. Cutoffs were set for the absolute value of the log fold change >0.25 between the two compared groups and percent of cells expressing the gene in at least one of the groups set >10%. Uniform Manifold Approximation and Projection was used to reduce the PCs to two dimensions for data visualization using the RunUMAP function.

Cell-type identification

Following PCA and UMAP, we analyzed cluster-specific differential gene expression. Marker genes were identified based on cluster-specific differential gene expression. For this purpose, for each gene we calculated the fraction of cells within the cluster that expressed the gene (referred to in Data S1 as pct1) and the fraction of cells outside the cluster that expressed the gene (referred to in Data S1 as pct2), and ranked genes by the ratio of pct1:pct2. Genes with high pct1:pct2 ratio and high pct1 values were selected as leading cluster-specific markers. The expression patterns of these genes were then examined in publicly available scRNA-seq data describing gene expression during mouse development[66] and in our prior published mouse medulloblastoma scRNA-seq studies,[11,37,50] to identify cell types.

Statistical analysis of IF data

Counts of total cells in tumor sections of counts of cells expressing each marker under study were analyzed using Microsoft Excel. Statistical tests used are specified in the results section.